Microwave Tomography for Industrial Process Imaging

DOI:
10.1109/MAP.2017.2731201

Document Version
Accepted author manuscript

Microwave Tomography for Industrial Process Imaging

Zhipeng Wu, *Senior Member, IEEE*, and Haigang Wang, *Member, IEEE*

***Abstract*--- This paper describes the implementation of microwave tomography for industrial process applications. Microwave tomography for industrial process imaging has different requirements from that for medical imaging. In addition to spatial resolution, high temporal resolution or real-time imaging is also important for high speed processes, flows or rapid reactions. Depending on the specific application, both quantitative imaging and qualitative imaging may be needed. Qualitative imaging would be sufficient to display distributions, patterns or shapes, which may be adequate for some applications. Quantitative imaging would however be more informative, giving images with quantitative dielectric contrast or permittivity values from which other physical parameters such as density, moisture content and phase fraction may be derived. With the microwave tomography approach described, several example applications in industrial processes are demonstrated, and a number of experimental imaging results are presented.**

Keyword---**microwave tomography, microwave imaging, instrumentation, image reconstruction**

I. Introduction

Tomographic imaging is a technique that reconstructs the internal distribution of an object in terms of a physical parameter and presents it as an image with a grey or color scale for easy visualization. Instead of a single point measurement, it offers a unique imaging method to the oil, chemical, pharmaceutical and food industries to visualize industrial processes without invading the pipes and vessels and provide valuable information for control and optimization. Since the concept of tomographic imaging was put into practice in the 1970's [1, 2], there has been a significant development in tomography instruments based on X-ray, γ-ray, magnetic resonance, optical, positron emission, ultrasound, electrical resistance, electrical capacitance, electromagnetic induction and microwaves [3, 4]. Among them, X-ray and magnetic resonance tomographic imaging instruments, which are often known as X-ray CT and MRI respectively, have been widely used in the medical sector. X-ray CT, MRI and optical tomography can all produce images of high spatial resolution. But X-ray CT is only applicable to the imaging of objects with large density contrast. MRI is only useful for imaging objects which contain water or hydrogen atoms. Optical tomography is applicable only to optically transparent substances or gases where optical attenuations are measureable. X-ray, MRI and optical instruments are all bulky and have therefore not found applications in industrial imaging. Positron emission and γ-ray imaging techniques can also produce high resolution images, but both involve the use of radiative tracer particles or ionizing radiation. They are therefore not welcome in the industrial environment.

On the other hand, electrical resistance and electrical capacitance tomographic techniques, which are often referred to as ERT and ECT respectively, have been applied to the imaging of industrial processes either in vessels or pipelines. ERT and ECT instruments are generally portable, but both have their application limitations. ERT is based on resistance measurements and is only applicable to the imaging of conducting substances. ECT is based on capacitance measurement and is only applicable to the imaging of non-conducting substances. Similarly, electromagnetic induction tomography (MIT) is applicable to the imaging of ferrous substances or conducting media. The images produced by ERT, ECT and MIT are of low spatial resolution. Ultrasound tomography is applicable to the imaging of substances with good acoustic properties, which usually involves liquids or solid-liquid mixtures. The images produced by ultrasound tomography are also of low spatial resolution.

Comparing to the tomographic imaging techniques above, microwave tomography is based on the measurements of the scattered electromagnetic fields produced by an object, and generates images of dielectric properties. The development of microwave tomography systems could be dated back to the late 1970's and early 1980's [5, 6]. Since then, there have been a significant number of papers published in the literature on the subject. The achievements, difficulties and challenges in the development of microwave tomographic imaging techniques, algorithms and systems over three decades to 2010 have been reviewed in the article by Bolomey and Jofre [7]. A total of 84 key publications on the subject during the period have been cited in this article. These are not to be repeated here. The readers are therefore referred to [7] for further information.

Over the past three decades, most of the microwave tomography research has been focused on medical and biomedical applications [8-30]. Only a limited number of publications have been on microwave tomography for non-medical applications [31-41], but these are increasing.

This manuscript was first submitted in July 2016 and revised in January 2017 and June 2017.

Zhipeng Wu* is with School of Electrical and Electronic Engineering, The University of Manchester, Manchester M13 9PL UK. (email: zhipeng.wu@manchester.ac.uk)

Haigang Wang is Institute of Engineering Thermophysics, Chinese Academy of Sciences, Beijing 100190, China.

Recent advances and new challenges in microwave tomographic imaging have been highlighted in [4], particularly in the aspect of real-time microwave tomography systems for industrial process monitoring applications.

Microwave tomography for industrial imaging has different requirements from that for medical imaging. In addition to spatial resolution, high temporal resolution or real-time imaging is also important for fast changing processes such as multiphase flows. Depending on the specific application, quantitative imaging and qualitative imaging are both needed. The former may be sufficient in many applications for displaying distributions, patterns or shapes. The latter would be more informative, giving images with quantitative dielectric contrast or permittivity values from which other physical parameters such as density, moisture content and phase fraction may be derived. In this paper, following the description of a microwave tomography system including the hardware and techniques for solving forward and inverse problems in Section II, example applications of the system in industrial process monitoring are demonstrated in Section III, together with the presentation of some experimental imaging results obtained. We aim to demonstrate the capability of a microwave tomography system for industrial applications mentioned above, but not to emphasize a new method or algorithm for image reconstruction.

II. The Microwave Tomography Imaging System

The basic principle of microwave tomography is to reconstruct the image of an object in terms of dielectric properties, such as dielectric constant ε_r or dielectric contrast s, from the data of the scattered microwave field measured around the object with microwaves incident from different angles creating multi-views of the object. To realize the microwave tomographic imaging, it requires the hardware for multi-view data acquisition and image display, and the technique for image reconstruction [4]. The hardware for microwave tomography system may include the circuits for microwave signal generation and detection, antennas for microwave signal transmitting and receiving, and a PC. The antennas are usually placed in a background medium, which could be a matching medium or natural air. A microwave tomography system developed for industrial process imaging is presented below.

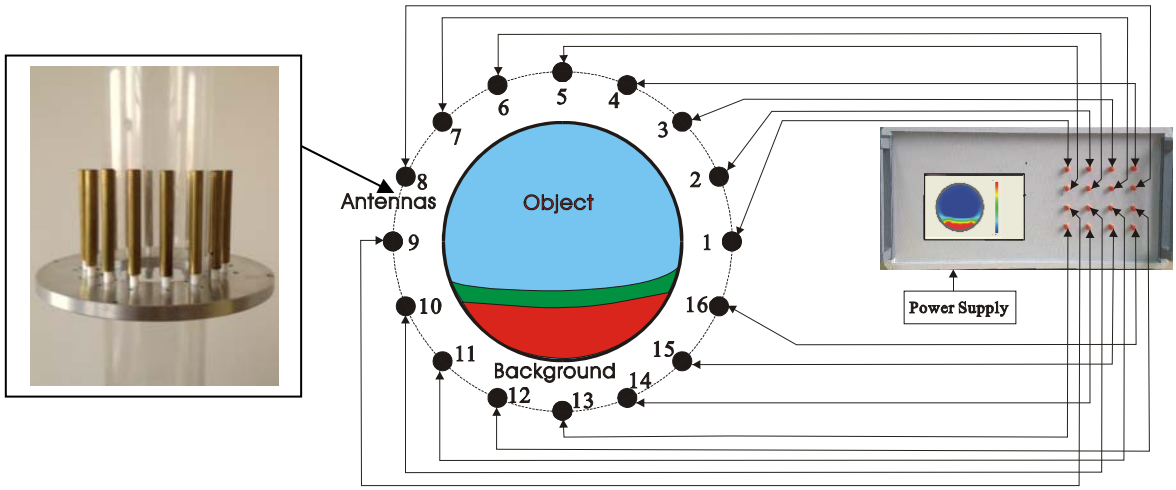

Fig.1 Diagram of the microwave tomography system

A. System Setup

The microwave tomography system setup used in this paper is shown in Fig.1. It uses 16 monopole antennas arranged in a circular configuration around the object being imaged in air. An example setup of the antennas around a circular acrylic pipe is shown in the photo inserted in Fig.1. A VCO is used for microwave generation, and a voltage is applied to set the operating frequency to be 1GHz with an output power of 10dBm. A different operating frequency may be obtained by varying the applied voltage. Amplitude and phase detectors are employed for measurements, serving similar functions to a vector network analyser [41]. A 2x16 multiplexer is implemented for the control of microwave transmission. The measurement scheme adopted in the system is to set each of the 16 monopole antennas as a transmitting antenna in turn and assign the remaining 15 monopole antennas as receiving antennas, with each measurement taking less than 0.2ms. This creates a set of 240 transmit-receive combinations with the measured scattered electric fields, $E_{t,m}^{s,meas} = E_{t,m}^{obj,meas} - E_{t,m}^{inc,meas}$, where t=1, 2…T and m=1, 2…M with T=16 and M=15, $E_{t,m}^{obj,meas}$ and $E_{t,m}^{inc,meas}$ are the total electric fields in the presence and absence of the object respectively. The system is therefore first calibrated with 240 transmit-receive measurements in the absence of object. Due to the reciprocity, only one half of the 240 transmit-receive combinations are independent. These measured scattered electric fields are used as the experimental data for image reconstruction.

The techniques for image reconstruction which involve solving both forward and inverse microwave scattering problems are described below.

B. Technique for Solving the Forward Scattering Problem

The microwave scattering by the object is generally a 3D scattering problem [42-44]. However, for simplicity, a 2D approximation is adopted [45, 46]. In the 2D model, the object is assumed to have no variation in its relative dielectric permittivity ε_r along its axis, and the antennas are modeled as line antennas. When the t-th antenna radiates, all other antennas are considered to be absent. In addition, the object is considered to have a circular cross-section and its diameter is taken as a priori knowledge. The 2D model is a compromise between the accuracy and computation time in solving the forward scattering problem or a compromise between the image quality and temporal resolution in solving the inverse scattering problem, which are both important for industrial process imaging.

In the 2D-model, the scattered electric field at any point r on the cross-section of the object, i.e. **Ω,** located on the same cross-sectional plane as the antenna due to the presence of the object can be expressed as [42, 47]:

$$E_t^s(r) = -k_0^2 \iint_{\Omega} s(r')E_t(r')G_{2D}(k_0\rho)dr' \tag{1}$$

where the subscript t indicates the radiation from the t-th antenna, r' is a point on Ω, $s(r') = \varepsilon_r(r')-1$ is the dielectric contrast at r', $G_{2D}(k_0\rho) = (j/4)\, H_0^{(2)}(k_0\rho)$ is the 2D Green's function with $\rho=|r-r'|$, and $E_t(r')$ is the total electric field at r'. The total electric field at any point r, including r' and measurement points r_m, is given by,

$$E_t(r) = E_t^{inc}(r) + E_t^s(r) \tag{2}$$

where $E_t^{inc}(r)$ is the incident electric field in the absence of the object. In the 2D-model, $E_t^{inc}(r)$ takes the form:

$$E_t^{inc}(r) = A_t H_0^{(2)}(k_0 r) \tag{3}$$

where A_t is a constant and related to the current on the t-th line antenna. In bridging the factorial difference between the theoretical model and experiment, A_t is chosen so that $E_t^{inc}(r_m) = E_{t,m}^{inc,meas}$ with t=1,2…T and m=1,2…M.

For a numerical solution, the cross-section of the object is divided into N=4197 cells. The n-th or n'-th cell, where n refers to the cell as a field point and n' as a source point, has an area of an equivalent radius of $a_{n'}$ [45] and dielectric contrast $s_{n'}$. In applying the Method of Moments to the discretised domain, Eqn. (1) above for the radiation from the t-th antenna is transformed to a matrix solution,

$$[E_m^s]_t = -[Z_{mn'}]_t[s_{n'}E_{n'}]_t = -[Z_{mn'}]_t[diag(s_{n'})][E_{n'}]_t \tag{4}$$

where $[E_m^s]_t$ is a Mx1 vector formed of the scattered electric fields at receiving positions, $[E_{n'}]_t$ is an Nx1 vector formed of the total electric fields at the discretised cells with n'=1,2…N, $[diag(s_{n'})]$ is a diagonal matrix of NxN formed of the dielectric contrasts at n'=1, 2…N, and $Z_{mn'}$ is given by,

$$Z_{mn'} = \frac{jk_0\pi a_{n'}}{2} J_1(k_0 a_{n'}) H_0^{(2)}(k_0\rho_{mn'}) \tag{5}$$

With the consideration of $[E_n]_t = [E_{n'}]_t$, the disretisation of Eqn.(2) leads to

$$\begin{aligned}[E_n^{inc}]_t &= [E_n]_t + [Z_{nn'}][s_{n'}E_{n'}]_t \\ &= ([I]+[Z_{nn'}][diag(s_{n'})])[E_{n'}]_t \end{aligned} \tag{6}$$

where $[E_n^{inc}]_t$ is an Nx1 vector formed of the incident electric fields at discretised cells, i.e. $E_t^{inc}(r_n)$, with n=1,2…N, [I] is an NxN unit matrix, the elements of $[Z_{nn'}]$ are given by [45],

$$Z_{nn'} = \begin{cases} \dfrac{jk_0\pi a_{n'}}{2} J_1(k_0 a_{n'}) H_0^{(2)}(k_0\rho_{nn'}) & if\ \ n \neq n' \\ \dfrac{jk_0\pi a_{n'}}{2} H_1^{(2)}(k_0\rho_{nn'}) & if\ \ n = n' \end{cases} \tag{7}$$

Hence,

$$[E_{n'}]_t = ([I]+[Z_{nn'}][diag(s_{n'})])^{-1}[E_n^{inc}]_t \tag{8}$$

and

$$[E_m^s]_t = -[Z_{mn'}]_t[diag(s_{n'})]([I]+[Z_{nn'}][diag(s_{n'})])^{-1}[E_n^{inc}]_t \tag{9}$$

Assuming the distribution of dielectric contrast $s_{n'}$ is known, the calculated scattered electric field at the position of the m-th receiving antenna for the t-th transmitting antenna would be $E_{t,m}^s$ which corresponds to the measured data $E_{t,m}^{s,meas}$ with t=1,2…T and m=1,2…M.

A study of a dielectric object with a uniform ε_r changing from 2 up to 90 shows that the numerical solution would be accurate only if the diameter of the discretised cells, i.e. $2a_{n'}$, is less than one tenth of the wavelength in the dielectric object (λ_ε) [48], indicating that the number of cells should be at least 100 per λ_ε x λ_ε area. It should be noted that an accurate forward solution is very important in an iterative method for solving inverse problems, particularly in high contrast cases.

C. Technique for Solving the Inverse Scattering Problem

To-date there have been a good number of algorithms developed for tomographic image reconstruction including both Born-based methods and iterative methods [8, 42, 49-61]. Iterative image reconstruction algorithms based on Gauss-Newton method [52], Newton-Kantorovich method [50, 51], quasi-Newton method [53], Conjugate gradient method [60, 61] and sequential quadratic programming method [55] have all been applied in microwave tomography. These methods would have different complexity, give different rates of convenience in the iterative process, produce images of different qualities, and have different levels of sensitivity to the quality of data. Some comparisons between the methods have been made in [54, 55]. For practical applications, a compromise between the factors may need to be made. In the following, an improved Newton-Kantorovich is described.

The method is chosen for simplicity and effectiveness. Other methods mentioned above may also be used.

C.1 Conventional Newton-Kantorovich Method

With the consideration of a small increment in the dielectric contrast distribution $[\delta s]=[\delta s_{n'}]$ in the conventional Newton-Kantorovich approach [50, 51], the differentiations of Eqn.(4) and Eqn.(6) lead to two incremental equations respectively,

$$[\Delta E_m^s]_t \approx -[Z_{mn'}]_t[\Delta(s_{n'}E_{n'})]_t \tag{10}$$

and

$$[\Delta E_n]_t \approx -[Z_{nn'}][\Delta(s_{n'}E_{n'})]_t \tag{11}$$

Eliminating $[\Delta(s_{n'}E_{n'})]_t$ gives,

$$[\Delta E_m^s]_t = [Z_{mn'}]_t[Z_{nn'}]^{-1}[\Delta E_n]_t \tag{12}$$

As $[Z_{mn'}]_t$ and $[Z_{nn'}]_t$ depend on the geometrical structure of the system setup, Eqn.(12) indicates that any difference in the calculated scattered electric field from its measured value is directly linked to the error in the calculated electric field inside the object. Eqn.(12) could be rearranged to,

$$[\Delta E_n]_t = [Z_{nn'}][Z_{mn'}]_t^{-1}[\Delta E_m^s]_t \tag{13}$$

Equation (13) shows that amount of correction required in the internal electric field in order to meet the difference between the calculated and measured electric fields. With the approximation of

$$[\Delta(s_{n'}E_{n'})]_t \approx [diag(E_{n'})_t][\Delta s_{n'}] + [diag(s_{n'})][\Delta E_{n'}]_t \tag{14}$$

in the conventional Newton-Kantorovich method [50, 51], it can be shown that

$$[\Delta E_m^s]_t = [D]_t[\Delta s_{n'}] \tag{15}$$

where

$$[D]_t = -[Z_{mn'}]_t([I]+[diag(s_{n'})][Z_{nn'}])^{-1}[diag(E_{n'})]_t \tag{16}$$

with [I] being the unit matrix. Eqn.(15) shows the relation between the variation of the dielectric contrast and that of the scattered electric field, or the resulted difference in the scattered electric field from the error in the dielectric contrast for each transmitting antenna t=1,2…T.

Assuming $[s_k]=[s_{n'}]_k$ is the approximate solution of s at the iterative step k, where k=0,1,2…K, an increment $[\delta s_k]=[\delta s_{n'}]_k$ would need to be added to form a new approximate solution of s at step k+1, i.e.

$$[s_{k+1}] = [s_k] + [\delta s_k] \tag{17}$$

The increment $[\delta s_k]$ at the k-th iteration can be found from

$$[D(s_k)][\delta s_k] = [\Delta E^s]_k \tag{18}$$

where

$$[\Delta E^s]_k = \begin{bmatrix} [\Delta E_m^s]_{t=1} \\ [\Delta E_m^s]_{t=2} \\ ..... \\ [\Delta E_m^s]_{t=T} \end{bmatrix}_k = \begin{bmatrix} [E_{1,m}^{s,meas} - E_{1,m}^s(s_k)] \\ [E_{2,m}^{s,meas} - E_{2,m}^s(s_k)] \\ ..... \\ [E_{T,m}^{s,meas} - E_{T,m}^s(s_k)] \end{bmatrix} \tag{19}$$

and

$$[D(s_k)] = \begin{bmatrix} [D(s_k)]_{t=1} \\ [D(s_k)]_{t=2} \\ ..... \\ [D(s_k)]_{t=T} \end{bmatrix} \tag{20}$$

with $[D(s_k)]_t$ given in Eqn.(16), i.e.

$$[D(s_k)]_t = -[Z_{mn'}]_t([I]+[diag(s_k)][Z_{nn'}])^{-1}[diag(E_{n'}(s_k))]_t \tag{21}$$

and $[E_{t,m}^s(s_k)]$ given in Eqn.(9), i.e.

$$[E_{t,m}^s(s_k)] = -[Z_{mn'}]_t[diag(s_k)]([I]+[Z_{nn'}][diag(s_k)])^{-1}[E_n^{inc}]_t \tag{22}$$

Equation (18) is generally ill-posed. It may be solved using various methods including singular value decomposition and Lavenberg-Marquardt (LM) method [62]. The application of LM method [62, 51, 52] with Tikhonov regularization [63] leads to the solution,

$$[\delta s_k] = [G(s_k,\alpha)][\Delta E^s]_k \tag{23}$$

with

$$[G(s_k,\alpha)] = ([D^*(s_k)][D(s_k)] + \alpha[I])^{-1}[D^*(s_k)] \tag{24}$$

where $[D^*(s_k)]$ is the conjugate transpose of $[D(s_k)]$ and α is the regularization parameter. A typical value of $\alpha=10^{-4}$ is adopted.

C.2 Improved Newton-Kantorovich Method

In the Newton-Kantorovich method above, $[D(s_k)]_t$ in Eqn.(21) involves the computation of $[E_{n'}(s_k)]_t$ using Eqn.(8) which is then re-arranged to form $[diag(E_{n'}(s_k))]_t$. However, the difference between the calculated and measured scattered electric fields in Eqn.(13) indicates that a better approximation to the calculated scattered electric field would be,

$$\begin{aligned}[E_{n'}^{'}(s_k)]_t &= [E_{n'}(s_k)]_t + [\Delta E_{n'}(s_k)]_t \\ &= [E_{n'}(s_k)]_t + [Z_{nn'}][Z_{mn'}]_t^{-1}[\Delta E_m^s(s_k)]_t \end{aligned} \tag{25}$$

Hence, the accuracy of $[D(s_k)]_t$ and the speed of reconstruction could be improved by replacing it with

$$[D_1(s_k)]_t = -[Z_{mn'}]_t([I]+[diag(s_k)][Z_{nn'}])^{-1}[diag(E^{'}_{n'}(s_k))]_t \quad (26)$$

The improved Newton-Kantorovich method gives an alternative equation for $[\delta s_k]$ as,

$$[D_1(s_k)][\delta s_k] = [\Delta E^s]_k \quad (27)$$

The application of LM method [62] with Tikhonov regularization [63] again leads to the solution,

$$[\delta s_k] = [G_1(s_k,\alpha)][\Delta E^s]_k \quad (28)$$

with

$$[G_1(s_k,\alpha)] = ([D_1^*(s_k)][D_1(s_k)] + \alpha[I])^{-1}[D_1^*(s_k)] \quad (29)$$

where $[D_1^*(s_k)]$ is the conjugate transpose of $[D_1(s_k)]$. The improved Newton-Kantorovich method is an iterative approach. The relative dielectric permittivity of the background medium is chosen as the initial guess. The iterative process is set to terminate when

$$Err = \| \Delta E^s \|_k^2 / \| E^{s,meas} \|^2 < 1\% \quad (30)$$

The improved Newton-Kantorovich method is suitable for both low and high contrast cases. However, the rate of convergence becomes slower as the contrast increases. The iterative process may also become divergent when the data contains high noise. In this case, the iterative process may be terminated after a small, but fixed number of iterations. Such enforcement would generally lead to qualitative imaging reconstruction only. Its improvement over the conventional Newton-Kantorovich method can be seen from the theoretical study shown in Fig.2 for the image reconstruction of a typical dielectric object with a diameter of 10cm and uniform ε_r=2. Qualitative reconstruction may be made in several iterations, which may be sufficient for some applications.

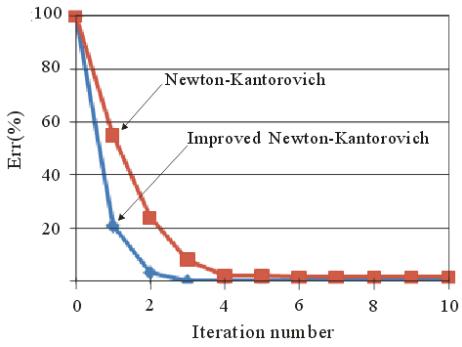

Fig.2 Err parameter of the reconstruction of a 10cm diameter object with ε_r=2 against the iteration number

III. Examples of Industrial Process Imaging

In this section, some potential applications of microwave tomography for industrial process imaging are illustrated. This is demonstrated experimentally using several practical imaging examples. As the substances involved have low conductivity or dielectric losses, the dielectric contrast and relative permittivity are dominated by real parts. Hence, only real value images are presented. As a result of 2D approximation, the images obtained represent the average dielectric properties in the axial direction in the case that there is an axial variation.

A. Imaging of Granule Substance in Different Flow Patterns

One application of the microwave tomography system is the imaging of solid or granule flows in a pipeline. Pneumatically conveyed solid or granule flows often occur in food, chemical, pharmaceutical industries and also in coal-fired power plants. Figure 3 shows the imaging of granules in three typical flow patterns. The granule substance is statically placed in a circular plastic pipe of 15cm in diameter. It is made of dry corn granules of sizes between 500μm and 2000μm and water by means of weighing and mixing to obtain required moisture of m_w=15% in weight. The dielectric constant of dry corn granules has a typical value of 1.8 [64], while the dielectric constant of the wet corn granule substance depends on its moisture which may be estimated using mixing formulas with $\varepsilon_{r,water}$=80 [65, 66]. Dielectric properties of grains and agricultural products may also be found in the work by Nelson et al. [67-69].

The first flow pattern has a flat boundary between the granule substance and air as shown in Fig.3(a). The granule substance in red occupies one half of the pipe cross-section with a 35^0 tilt angle, and air occupies the remaining area. The reconstructed image of the corresponding flow pattern in terms of the normalized dielectric contrast $s/s(m_w=15\%)$ is shown in Fig.3(b) where $s(m_w=15\%)$ is the dielectric contrast of the formulated granule substance with a moisture content of m_w=15%. By choosing the normalized dielectric contrast function to plot, the variation of the dielectric property is mapped to the range between zero and unity. In Fig.3(b), the reconstructed area of granule substance is represented and shown in red with a normalized dielectric contrast of unity, and the area of air in blue with a normalized dielectric contrast of zero. The tilt angle can be clearly seen from the reconstructed image. The second flow pattern has the granule substance (red) distributed at the centre of the pipe and surrounded by air (blue), as shown in Fig.3(c). Its corresponding reconstructed image in terms of $s/s(m_w=15\%)$ is shown in Fig.3(d). The concentration of the granule substance towards the centre of the pipe can be seen from the image, but the centre of the granule concentration is slightly off the centre of the pipe. This deviation from the model reflects the actual position of the granules in the experiment. The third flow pattern has a large air bubble column (blue) embedded in the granule substance which occupies a majority of the pipe cross-section, as shown in Fig.3(e). The reconstructed image of the flow pattern in terms of $s/s(m_w=15\%)$ is shown in Fig.3(f). The position and size of the air bubble can be seen from the reconstructed image. These examples show that qualitative imaging of flow patterns may be made using the microwave tomography system.

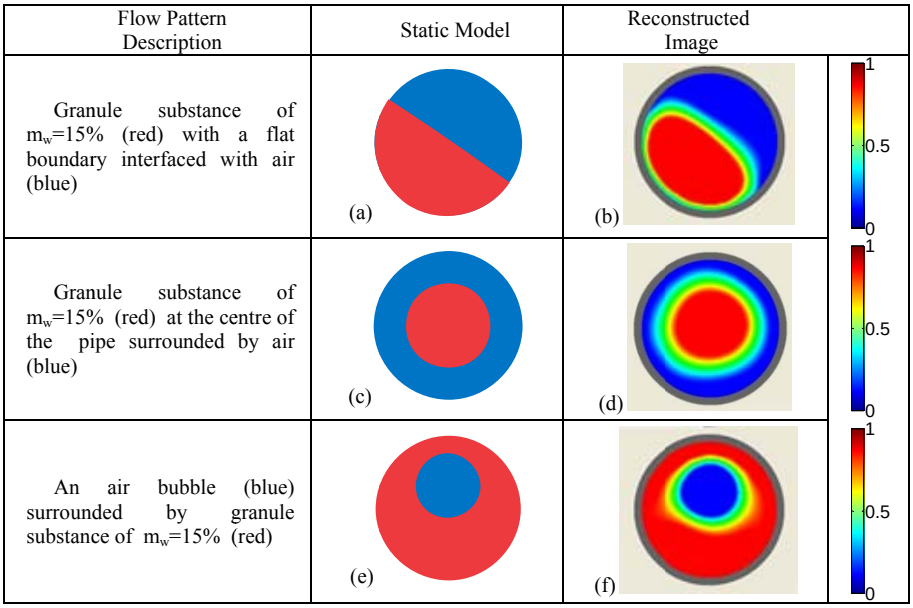

Fig.3 Image reconstruction of three typical flow patterns: (a) Granule substance with a flat boundary interfaced with air, (b) Granule substance at the centre of the pipe surrounded by air (blue), and (c) an air bubble surrounded by granule substance. The granule substance has m_w=15%.

B. Imaging of Granule Substances with Different Moisture Contents

A further investigation from above is to include different granule substances. Figure 4 shows the imaging of corn granule substances of different moisture contents with the flat granule-air boundary model as shown in Fig.4(a). The pipe remains the same as above. The formulated granule substances are have a moisture content of m_w=10%, 20% and 30% respectively. The granule substance in red occupies approximately one half of the pipe cross-section with a 35^0 tilt angle in the model, and air occupies the remaining area. The reconstructed images for these three cases in terms of the normalized dielectric contrast s/s(m_w=10%), s/s(m_w=20%) and s/s(m_w=30%) are shown in Figs.4(b)-(d) respectively, all with values in the range between 0 and 1, where s(m_w=10%), s(m_w=20%), and s(m_w=30%) are the dielectric contrasts of the formulated granule substances with moisture contents of m_w=10%, m_w=20% and m_w=30% respectively. In each image, the reconstructed area of its corresponding granule substance is shown in red with a normalized dielectric contrast of unity, and the area of air in blue with a normalized dielectric contrast of zero. The tilt angle can be seen from all three reconstructed images. However, the reconstructed image for m_w=30% has a slightly larger tilt angle. This difference from the model reflects the actual position of the granule substance at the experiment. It also shows the effectiveness of the microwave tomography system in differentiating the angular variation of the object being imaged as well as the dielectric contrast.

Figure 5 shows the imaging of corn granule substances with moisture contents of m_w=10%, 20% and 30% with a distribution model shown in Fig.5(a). The pipe is the same as above. The reconstructed images are presented in the form of $f(\varepsilon_r)=(\varepsilon_r-1)/\varepsilon_r(m_w=10\%)$, taking the relative permittivity $\varepsilon_r(m_w=10\%)$ as the denominator for normalization, so that $f(\varepsilon_r=1)=0$ in the case of air represented in blue. The reconstructed images for the granule substances with m_w=10%, 20% and 30% are shown in Figs.5(b), (c) and (d) respectively. The use of the color scheme not only shows the locations of the granule substances, but also gives the level of the relative permittivity. A comparison between Figs.5(b), (c) and (d) shows that as the moisture content increases, the relative permittivity increases. This can be clearly seen from the images. The capability of the microwave tomography system as a tool for qualitative imaging is again illustrated.

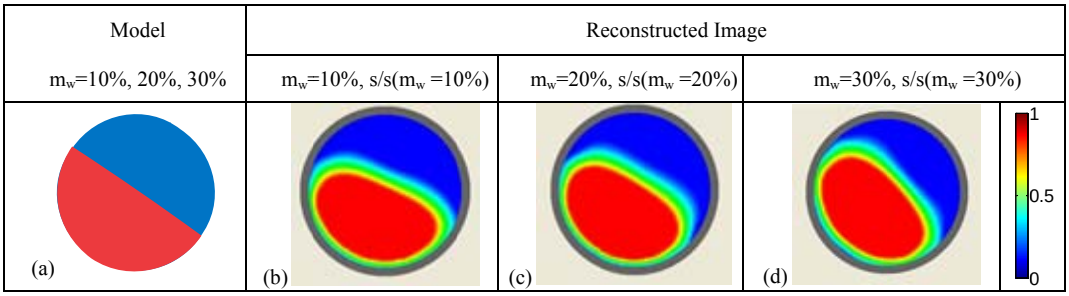

Fig.4 Image reconstruction of granule substances with a flat boundary interfaced with air and three different moisture contents: (a) the distribution model, (b) m_w=10%, (c) m_w=20% and (d) m_w=30%.

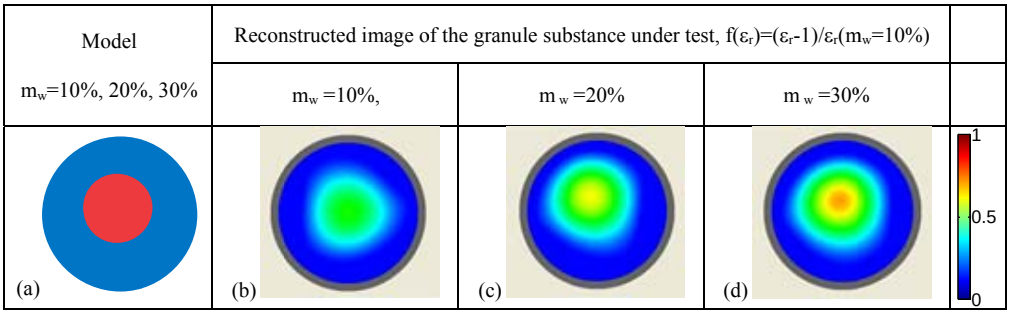

Fig. 5 Reconstruction images of granule substances with moisture contents presented in the form of $f(\varepsilon_r)=(\varepsilon_r-1)/\varepsilon_r(m_w=10\%)$: (a) the distribution model, (b) m_w=10%, (c) m_w=20% and (d) m_w=30%

Should the effective relative constant values of the granule substances are obtained from the images in Figs.5(b), (c) and (d) to provide quantitative imaging, the value for m_w=10% is approximately 2.22, and those for m_w=20% and 30% are approximately 2.44 and 2.67 respectively. Their corresponding values from the corn-water two-substance mixing formula are 2.4, 3.4 and 4.7 respectively [65, 66]. The differences come from at least three sources: (i) the system' error in providing accurate relative dielectric constant values, (ii) an error resulted from the approximation of the mixing formula, (iii) the fact that the object is not a corn-water two-substance mixture, but a corn-water-air three-substance mixture where the air voids can contribute to make the effective dielectric constant lower. While the exact sources of error are uncertain, from the engineering point view, the imaging in Figs.5(b), (c) and (d) can be taken as calibrations or system's learning to establish an experimental relation between the appearing dielectric constant and moisture content for this specific application, as shown in Fig.6. This curve would be sufficient to monitor the moisture content of corn granules in a drying process from the images obtained and estimate its moisture content in the range between 30% and 0%.

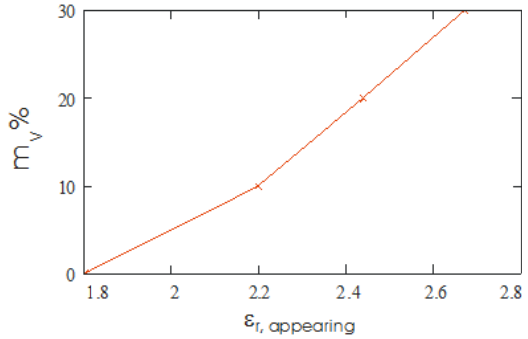

Fig. 6 Experimental relation between the appearing dielectric constant and moisture content

C. *Imaging of Powder Flow in a Pipe*

Figure 7 illustrates the imaging of powder flow in a horizontal plastic pipe of 3cm in diameter. The powder is made of dry wheat flour. It has a dielectric constant ε_r=1.6 approximately [64], and flows from right to left. The imaging position, where the microwave tomography system is placed, is at the right-end of Fig.7(a). Images are produced continuously one after the other [70]. As time progresses, a total of 200 images including Figs.7(b)-(g) are obtained, and they are stacked up to form a 3D image with the 1st image on the most left and the 200th image on the most right which maps the direction of flow. A physical mapping between the image number and the actual position from the right-end of the pipe could be made if the flow speed is known. The stacked 3D image could give a direct view of flow variation in time. For instance, by taking a vertical cut along the centre axis of the stacked 3D image, a density distribution on the corresponding vertical plane of the pipe along the centre axis can be observed, as shown in Fig.7(a) where a color scale is adopted so that red indicates the 100% occupation of the powder and blue 0% occupation. The imaging results indicate that the powder flows initially with a varying but low density across the whole pipe cross-section (Figs. 7(b) and (c)). It then stops (Fig.7 (d)). This is followed by an increased amount of powder flow with powder concentrating at the bottom part of the horizontal pipe and dispersing upwards (Fig. 7(e)). The powder flow stops again before a larger amount of powder flows which occupies almost 50% of the pipe cross-section on the bottom part of the pipe (Figs. 7(f) and (g)). For qualitative imaging, the characteristics of flow can be observed from these images. For quantitative imaging, the density of the powder flowing in the pipe could be estimated from the dielectric contrast shown on the image. It is noted that both flow pattern and quantity are important for industrial process control and optimization.

D. *Imaging of a Substance with State Change*

Some of the industrial processes may involve a substance that changes its physical state during the process. The physical state may change from solid to liquid, liquid to gas or vice versa as temperature or pressure varies. To demonstrate the observation of state change of a substance, a cylindrical ice column of 3cm in diameter shown in Fig.8(a) is used in imaging. The ice column with $\varepsilon_{r,ice}$=4 is placed into a horizontal plastic pipe of the same inner diameter at normal atmospheric pressure and room temperature. The pipe thickness is 1mm. The ice naturally melts into water with $\varepsilon_{r,water}$=80 as time elapses. Figures 8.(b)-(l) shows a selection of the images captured in the process during a period of 12 hours. The images are plotted in terms of $(\varepsilon_r-\varepsilon_{r,ice})/\varepsilon_{r,water}$ so that zero value or blue indicates ice state, red the water state, and any color

in-between the intermediate state or the mixture of water and ice.

Figure 8(b) is the image of the initial state of ice. Figure 8(c) shows that the ice starts to melt from the bottom left of the ice cross-section. It then progresses along the left side and bottom part of the ice cross-section and also towards the right side (Figs. 8(d)). The amount of ice melting progressively increases, and so is the amount of water (Figs. 8(e)-(h)) which naturally flows towards the bottom of the pipe. The amount of ice floating on the top part of the pipe cross-section progressively reduces (Figs. 8(i)-(k)). Figure 8(i) shows that only a small piece of ice remains at the stage of imaging, which floats on the top of the pipe cross-section. In Fig. 8(k) it shows that the ice has melted almost completely, and water occupies a major area of the pipe cross-section above the bottom with ice-water mixture on the remaining area. Figure 8(l) shows that the ice melts completely after 12 hours.

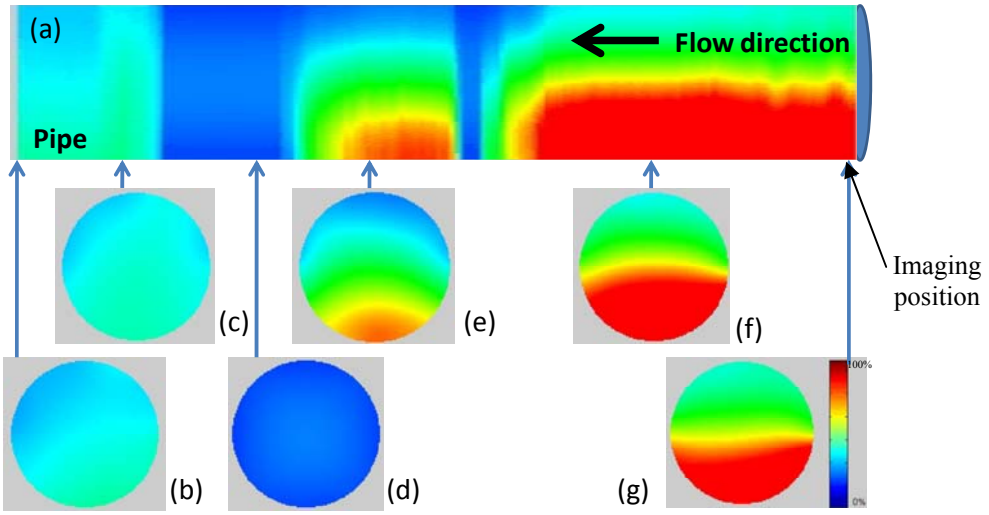

Fig. 7 Imaging of powder flow in a horizontal pipe

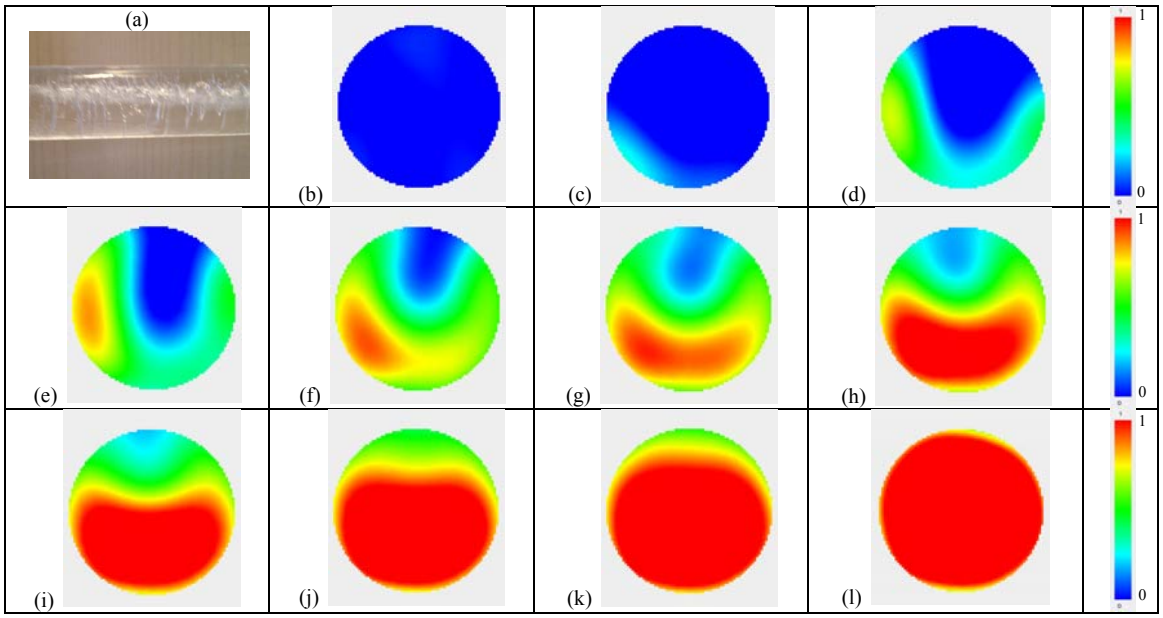

Fig. 8 Imaging of state change of ice (a) into water and selected images in sequence from (b) to (l)

IV. Discussion and Conclusions

Over the past three decades, there has been a significant development in microwave tomographic imaging techniques, algorithms and systems for medical scanning and industrial process monitoring applications. In this paper, we focus ourselves on the investigation of the latter. For medical imaging, to achieve high image quality or spatial resolution is the ultimate aim. The reconstruction time is of secondary importance. However, for industrial process imaging, high image quality and high temporal resolution are equally important, particularly for applications involving high speed processes, flows or rapid reactions, even though a compromise between them

may sometimes need to be made. Although the reconstructed images may be presented in colors with their corresponding quantitative dielectric contrast or permittivity values, qualitative images showing the distributions, patterns or shapes may be sufficient in many applications. Quantitative images would of course be more informative, from which other physical parameters such as density, moisture content and phase fraction may be further derived.

As a result of the development in microwave electronics in recent years, a microwave tomography system could be designed to be portable and produce high quality images in real time for process monitoring applications in oil, chemical, pharmaceutical and food industries. Example applications of the microwave tomography system for the imaging of granule substances, powder flow and state change of ice to water have demonstrated the potential of technology for these applications. As with other imaging modalities, it is envisaged that microwave tomography as a technique or a system will increasingly find its way into processing, manufacturing, packaging and other industrial sectors in the years to come to improve product quality, efficiency and productivity, coupled with the new developments in the Internet of Things, Industry 4.0 in Europe, and Made-in-China 2025 Initiative in China.

ACKNOWLEDGEMENT

Respectively the authors would like to thank all former colleagues, research associates and postgraduate students who had contributed to the study of microwave tomography at UMIST and the University of Manchester, the National Natural Science Foundation of China (No. 61320106004) and CAS Interdisciplinary Innovation Team for their supports. The authors would also like to thank Dr A. T. Nugroho for producing the results shown in Fig.2.

REFERENCES

[1] A. M. Cormack, "Reconstruction of densities from their projections, with applications in radiological physics," Physics in Medicine and Biology, Vol.18, No. 2, pp195–207, 1973.

[2] G. N. Hounsfield, "Computerized transverse axial scanning (tomography)—part 1. Description of the system," British Journal of Radiology, Vol.46, pp1016–1022, 1973.

[3] M. S. Beck, "Process tomography: a European innovation and its applications," Meas. Sci. Technol. Vol.7, pp215-224, 1996.

[4] Z. Wu, Developing a microwave tomographic system for multiphase flow imaging: advances and challenges, Transactions of the Institute of Measurement and Control, Vol. 19 September 2014 , DOI: 10.1177/0142331214546523.

[5] L. E. Larsen and J. H. Jacobi, "Microwave scattering parameter imagery of an isolated canine kidney," Med. Phys., Vol.6, pp394-403, 1979.

[6] J.-Ch. Bolomey, A. Izadnegahdar, L. Jofre, Ch. Pichot, G. Peronnet, And M. Solaimani, "Microwave diffraction tomography for biomedical applications," IEEE Transactions on Microwave Theory and Techniques, Vol.30, No.11, pp1998-2000, 1982.

[7] J.-Ch. Bolomey and L. Jofre, "Three decades of active microwave imaging achievements, difficulties and future challenges," in 2010 IEEE International Conference on Wireless Information Technology and Systems (ICWITS), p1-4, DOI:10.1109/ICWITS.2010.5611904.

[8] L. E. Larsen and J. H. Jacobi," Medical Applications of Microwave Imaging," IEEE Press, 1986

[9] L. Jofre, M. S. Hawley, A. Broquetas, E. de los Reyes, M. Ferrando, A. R. Elias-Fusté, L., "Medical Imaging with a microwave tomographic scanner," IEEE Transactions on Biomedical Engineering, Vol. 31, No.3, pp303-311, 1990

[10] S. Y. Semenov, R. H. Svenson, A. E. Boulyshev, A. E. Souvorov, V. Y. Borisov, Y. Sizov , A. N. Starostin, K. R. Dezern, G. P. Tatsis, V. Y. Baranov, "Microwave tomography: two-dimensional system for biological imaging," IEEE Transactions on Biomedical Engineering, Vol.43, No.9, pp869-877, 1996.

[11] P. M. Meaney, M. W. Fanning, D. Li, S. P. Poplack, K. D. Paulsen, "A clinical prototype for active microwave imaging of the breast," IEEE Transactions on Microwave Theory and Technology, Vol.48, No.11, pp1841-1853, 2000.

[12] P.M. Meaney, K. D. Paulsen, M. W. Fanning, "Microwave imaging for breast cancer detection: preliminary experience," Proc. SPIE—Int. Soc. Opt. Eng., Vol. 3977, 308-319, 2000.

[13] P. M. Meaney, K. D. Paulsen, B. W. Pogue, M. I. Miga, "Microwave image reconstruction utilizing log-magnitude and unwrapped phase to improve high-contrast object recovery," IEEE Trans. Med. Imag., Vol.20, pp104-116, 2001.

[14] P. M. Meaney, K. D. Paulsen, A. Hartov, R. K. Crane, "An active microwave imaging system for reconstruction of 2-D electrical property distributions," IEEE Trans. Biomed. Eng. Vol.42, No.10, pp.1017-1026, 1995.

[15] P. M. Meaney, K. D. Paulsen, A. Hartov, R. K. Crane, "Microwave imaging for tissue assessment: Initial evaluation in multitarget tissue-equivalent phantoms," IEEE Trans. Biomed. Eng., Vol.43, No.9, pp878-890, 1996.

[16] Meaney P. M., M. W. Fanning, R. M. di Florio-Alexander, P. A. Kaufman, S. D., T. Zhou, K. D. Paulsen, "Microwave tomography in the context of complex breast cancer imaging," in Conf Proc IEEE Eng Med Biol Soc. 2010; 3398-401. doi: 10.1109/IEMBS.2010.5627932.

[17] C. Pichot, L. Jofre, G. Peronnet and J. Bolomey, "Active microwave imaging of inhomogeneous bodies," IEEE Trans. Antenna Propagat. Vol.33, No.4, pp416-425, 1985.

[18] J. C. Bolomey and C. Pichot, "Microwave tomography: From theory to practical imaging system," Int. J. of Imaging System Technology, Vol.2, No.2, pp144-156, 1990.

[19] A. H. Golnabi, P. M. Meaney and K. D. Paulsen, "3D microwave tomography of the breast using prior anatomical information," Medical Physics, Vol.43, pp1934-44, 2016.

[20] F. Bai, A. Franchois and A. Pizurica, "3D microwave tomography with Huber regularization applied to realistic numerical breast phantoms," Progress In Electromagnetics Research, Vol. 155, pp75–91, 2016.

[21] S,-H. Son, H.-J. Kim, K.-J. Lee, J.-Y. Kim, J.-M. Lee, S.-I. Jeon, H.-D. Choi, "Experimental measurement system for 3–6 GHz microwave breast tomography," Journal of Electromagnetic Engineering and Science, Vol.15, No. 4, pp250-257, 2015.

[22] V. Zhurbenko, "Challenges in the design of microwave imaging systems for breast cancer detection," Advances in Electrical and Computer Engineering, Vol.11, No.1, p91-96, 2011.

[23] Q. Fang, P. M. Meaney and K. D. Paulsen, "Viable three-dimensional medical microwave tomography: theory and numerical experiments," IEEE Transactions on Antennas and Propagation, Vol. 58, No. 2, pp449-458, 2010.

[24] R. Chandra, H. Zhou, I. Balasingham and R. M. Narayanan, "On the opportunities and challenges in microwave medical sensing and imaging," IEEE Transactions on Biomedical Engineering, Vol. 62, No. 7, pp1667-1682, 2015,

[25] S. C. Hagness, E. C. Fear, A. Massa, "Guest Editorial: Special cluster on microwave medical imaging," IEEE Antennas and Wireless Propagation Letters, Vol. 11, pp1592-1597, 2012.

[26] S.-H. Son, N. Simonov, H.-J. Kim, J.-M. Lee and S.-I. Jeon, "Preclinical prototype development of a microwave tomography system for breast cancer detection," ETRI Journal, Vol.32, No.6, pp901-910, 2010.

[27] J.-Y. Kim, K.-J. Lee, S.-H. Son, J.-M. Lee, H.-J. Kim, B.-R. Kim, N. Simonov, S.-I. Jeon and N. Kim, "Design and preliminary experiments of a precision microwave tomography system," Microwave And Optical Technology Letters, Vol. 57, No. 10, 2015, 2445-2448.

[28] E. A. Attardo, A. Borsic, G. Vecchi and P. M. Meaney, "Whole-system electromagnetic modeling for microwave tomography," IEEE Antennas and Wireless Propagation Letters, Vol.11, pp1618-1621, 2012.

[29] A. Zakaria, A. Baran and J. LoVetri, "Estimation and use of prior information in fem-csi for biomedical microwave tomography," IEEE Antennas and Wireless Propagation Letters, Vol. 11, 1606-1609, 2012.

[30] M. Jalilvand, C. Wu, J. Schmid and T. Zwick, "Quantitative imaging of numerically realistic human head model using microwave tomography," Electronics Letters, Vol. 50, No. 4, pp. 255–256, 2014.
[31] C. Pichot, "Inversion algorithms and measurement systems for microwave tomography of buried objects," in Proceedings of the 16th IEEE Instrumentation and Measurement Technology Conference, 1999.
[32] C. Dourthe, "Inversion algorithm and measurement system for microwave tomography of buried object," Radio Science, Vol. 35, No.5, pp1097-1108, 2000.
[33] J.-Ch. Bolomey, "Recent European developments in active microwave imaging for industrial, scientific, and medical applications," IEEE Transaction on Microwave Theory and Techniques, Vol. 37, pp2109-2117, 1989.
[34] Z. Wu, H. McCann, L. E. Davis, J. Hu, A. Fontes and C. G. Xie, "Microwave tomographic imaging of oil and gas multiphase flows," in World Congress on Industrial Process Tomography, Beijing, China, 2010.
[35] Z. Wu, H. McCann, L. E. Davis, J. Hu, A. Fontes and C. G. Xie, "Microwave tomographic system for oil and gas multiphase flow imaging," Meas. Sci. Technol., Vol.20, No.10, 104026 (8pp), 2009.
[36] Z. Wu, A. Boughriet, H. McCann, L. E. Davis and A. T. Nugroho, "Investigation of microwave tomographic imaging techniques for industrial processes," in SPIE Conf. on Process Imaging for Automatic Control, Massachusetts, USA, pp151-158, 5-8 Nov. 2000.
[37] A. Boughriet, Z. Wu, A. T. Nugroho, H. McCann and L. E. Davis, "Free space imaging with an active microwave tomographic system," in SPIE International Conference on Subsurface Sensing Technologies and Applications II, 30 July - 4 Aug. 2000.
[38] E. R. Almeida, J. L. Porsani, I. Catapano, G. Gennarelli and F.Soldovieri, "Microwave tomography-enhanced GPR in forensic surveys: the case study of a tropical environment," IEEE Journal of Selected Topics in Applied Earth Observations and Remote Sensing, Vol.9, No. 1, pp115-124, 2016.
[39] C.Gilmore, M. Asefi, J. Paliwal and J. LoVetri, "Industrial scale electromagnetic grain bin monitoring," Computers and Electronics in Agriculture, Vol.136, pp210-220, 2017.
[40] M. Asefi, I. Jeffrey, J. LoVetri, C. Gilmore, P. Card, and J. Paliwal, "Grain bin monitoring via electromagnetic imaging," Computers and Electronics in Agriculture, Vol.119, pp133-141, 2015.
[41] Z. Wu, "Software VNA and Microwave Network Design and Characterisation, Wiley & Sons, April, 2007, ISBN: 978-0-470-51215-9.
[42] M. Pastorino, "Microwave Imaging," Wiley & Sons, 2010.
[43] J. Hu, Z. Wu , H. McCann, L. E. Davis, C. G. Xie, "Quasi-3D modeling of electromagnetic wave scattering of dielectric objects for microwave tomography," in 3rd World Congress on Industrial Process Tomography, p213-218, 2003.
[44] J. Hu, Z. Wu , H. McCann, L. E. Davis, C. G. Xie, " Quasi-three-dimensional method of moment for analyzing electromagnetic wave scattering in microwave tomography systems," IEEE Sensors Journal, Vol.5, No.2, pp216-235. 2005.
[45] J. Richmond, "Scattering by a dielectric cylinder of arbitrary cross section shape," IEEE Transactions on Antennas and Propagation, Vol.13, No.3, pp334-341, 1965.
[46] S. Caorsi, G. L. Gragnani, M. Pastorino, "Two-dimensional microwave imaging by a numerical inverse scattering solution," IEEE Transactions on Microwave Theory and Techniques, Vol.38, No.8, pp981-980, 1990.
[47] A. T. Nugroho and Z. Wu, "Inexact newton backtracking method for solving microwave tomography inverse problem," in IEEE International Conference on Imaging Systems and Techniques , Macao, 16-19 Sept 2015.
[48] A.T. Nugroho, "Microwave tomography", University of Manchester, 2015.
[49] W.C. Chew and Y. M. Wang, "Reconstruction of two-dimensional permittivity distribution using the distorted Born iterative method," IEEE Transactions on Medical Imaging, Vol.9, No.2, pp218-225, 1990.
[50] A. Roger, "A Newton Kantorovich algorithm applied to an electromagnetic inverse problem," IEEE Transactions on Antennas and Propagation, Vol. 29, No.2, pp 232-238, 1981.
[51] N. Joachimowicz, C. Pichot, J. P. Hugonin, "Inverse scattering: an iterative numerical method for electromagnetic imaging," IEEE Transaction on Antennas and Propagation, Vol.39, No.12, pp1742-1752, 1991.
[52] A. Franchois and C. Pichot, "Microwave imaging - Complex permittivity reconstruction with a Levenberg-Marquardt method," IEEE Transaction on Antennas and Propagation, Vol. 45, No. 2, pp 203-215, 1997.
[53] A. Franchois and A. G. Tijhuis, "A quasi-Newton reconstruction algorithm for a complex microwave imaging scanner environment," Radio Science, Vol. 38, No.2, pp8011-8023, 2003.
[54] J. Hu, Z. Wu, H. McCann, L. E. Davis, C. G. Xie, "BFGS Quasi-Newton method for solving electromagnetic inverse problems," IEE Proc. on Microwaves, Antennas and Propagation, Vol.153, No.2, pp199-204, 2006.
[55] J. Hu, Z. Wu, H. McCann, L. E. Davis, C. G. Xie, "Sequential quadratic programming method for solution of electromagnetic inverse problems," IEEE Trans. Antennas and Propagation, Vol. 53, No. 8, pp 2680-2687, 2005.
[56] Z. Wu, "Application of radio ground wave propagation theory to the tomographic imaging of ground surfaces," IEEE Transaction in Antennas and Propagation, Vol. 48, No.9, pp1384-1392, 2000.
[57] Z. Wu, "Tomographic imaging of isolated ground surfaces using radio ground waves and conjugate gradient methods," IEE Proceedings: Radar, Sonar and Navigation, Vol.148, No.1, pp27-34. 2001.
[57] Z. Wu, "Frequency and noise dependence of the image reconstruction of ground surfaces using the conjugate gradient based algorithm," IEE Proceedings: Radar, Sonar and Navigation Vol. 148, No.4, pp211-218, 2001.
[58] Z Wu., "Effects of noise and system's parameters on the tomographic image reconstruction of ground surfaces," IEEE Trans. On Antennas and Propagation, Vol.51, No.6, pp1401-1403, 2003.
[60] H. Harada, D. J. N. Wall, T. Takenaka, M. Tanaka, "Conjugate gradient method applied to inverse scattering problem," IEEE Transactions on Antennas and Propagation, Vol.43, No.8, pp784 -792, 1995.
[61] P. Lobel, R. E. Kleinman, Ch. Pichot, L. Blanc-Feraud, "Conjugate-gradient method for solving inverse scattering with experimental data," IEEE Antennas and Propagation Magazine Vol.38, No.3, pp48-51, 1996.
[62] P. Neittaanmaki, M. Rudnicki and A. Savini, "Inverse problems and optimal design in electricity and magnetism", Clarendon Press, Oxford, 1996.
[63] A. N. Tikhonov and V. S. Arsenin, "Solutions of ill-posed problems," John Wiley & Sons, London 1977.
[64]https://www.honeywellprocess.com/library/marketing/techspecs/Dielectric%20Constant%20Table.pdf
[65] A. Sihvola, "Mixing models for heterogeneous and granular Media", in "Advances in Electromagnetics of Complex Media and Metamaterials", edited by S. Zouhdi, et al., Kluwer, Amsterdam, 2002.
[66] T. Hanai, "Emulsion Science". Academic Press, NY. 1968.
[67] S. O. Nelson, A. W. Kraszewski, S. Trabelsi and K. C. Lawrence, C., "Using cereal grain permittivity for sensing moisture content," IEEE transactions on instrumentation and measurement, Vol.49, No.3, pp470-475, 2000.
[68] S. Nelson, "Dielectric Properties of Agricultural Materials and Their Applications, Academic Press, 2015.
[69] S. O. Nelson, "Dielectric properties of agricultural products and some applications," Res. Agr. Eng., Vol.54, No.2, pp104–112, 2008.
[70] https://www.youtube.com/watch?v=YIHuuv4lQcY

AUTHOR INFORMATION

Zhipeng Wu (zhipeng.wu@manchester.ac.uk) is a professor in the School of Electrical and Electronic Engineering, University of Manchester, UK. His research interests include antennas and propagation, microwave tomography, microwave sensors and instrumentation, IoT and applications.

Haigang Wang (wanghaigang@iet.cn) is a professor in the Institute of Engineering Thermophysics, Chinese Academy of Sciences, China. His research interests include multiphase flow measurement, CFD simulation and process tomography.